Anura3D
MPM Research Community

Paper number: mpm2019.54
www.anura3d.com
www.mpm2019.eu

A study of collapse in slopes using MPM and NLA (Numerical Limit Analysis)

Fabricio Fernández[1,*], Eurípedes Vargas Jr.[1], Raquel Quadros Velloso[1]
[1]Catholic University of Rio de Janeiro, Brazil

[*]E-mail:fabriciof@puc-rio.br

ABSTRACT

The material point method (MPM) and numerical limit analysis (NLA) are used for the study of collapse of two 3D slopes. The main objective of this work is to compare the results in terms of the slope safety factor and the collapse mechanism, for two analyzed cases. The first case is a heterogeneous two materials 3D slope. The second case is the experimental catchment in the Oregon Coast Range, which collapse was triggered by heavy rains. In both cases, elasto-plastics materials are considered, and the pore pressure effects are considered in a non-coupled way through the constitutive relations.

KEY WORDS: 3D slope stability; Material point method; Numerical limit analysis; Oregon Coast Range

INTRODUCTION

The evaluation of the risk of a slope failure requires at least a quantification of the stability conditions. The stability conditions can be determined from the slope safety factor (SF) and the probable collapse mechanism. The hypothesis of planes train in problems of complex geometries in 3D is not respected and the determination of (SF) must consider this condition. The objective of this work is to compare the results of the 3D slope stability analysis, in terms of the slope safety factor and the collapse mechanism, using two numerical methods. The material point method (MPM) and the numerical limit analysis (NLA) method are used for the study of the collapse of two slopes in 3D. The first case is a heterogeneous two materials slope. The second case is the experimental catchment in the Oregon Coast Range, which collapse was triggered by heavy rains. In both cases,elasto-plastic materials are considered, and the pore pressure effects are considered in a non-coupled way through the constitutive relations.The work is organized in the following way: First, the theory of NLA and MPM is presented briefly. Second, the results of the two cases analyzed are presented. And finally the conclusions.

NUMERICAL LIMIT ANALYSIS

The numerical limit analysis is based on finite element method and mathematical programming to determine the slope safety factor and the collapse mechanism. The limit analysis plasticity theorems are placed in the form of an optimization problem, which is formulated within the framework of second-order conic programming. The optimization problem thus formulated has shown to have computational efficiency in 3D models (Krabbenhøft et al., 2007; Makrodimopoulos and Martin, 2006).

The equilibrium equations are derived from the principle of virtual powers. Considering only the own weight as external force in the slope stability problem, the weak form of the equilibrium equation can be written as (Camargo et al., 2016):

$$\int_V \delta\dot{\boldsymbol{\varepsilon}}^T \boldsymbol{\sigma}\, dV = \int_V \delta\dot{\mathbf{u}}^T \mathbf{F}\, dV \tag{1}$$

where $\mathbf{F}$ is the body force due to the weight of the slope, $\dot{\boldsymbol{\varepsilon}}$ is the plastic strain rate tensor, $\dot{\mathbf{u}}$ is the velocity vector, and $\boldsymbol{\sigma}$ is the stress tensor.

The discrete form of the equilibrium equation (Equation 1) is obtained expressing the stress $\boldsymbol{\sigma}$ and velocity fields $\dot{\mathbf{u}}$ by interpolation functions $\mathbf{N}_\sigma$, $\mathbf{N}_\mathrm{u}$and nodal values $\hat{\boldsymbol{\sigma}}$, $\hat{\dot{\mathbf{u}}}$ of a finite element mesh.

$$\boldsymbol{\sigma} = \mathbf{N}_\sigma \, \hat{\boldsymbol{\sigma}} \tag{2}$$

$$\dot{\mathbf{u}} = \mathbf{N}_\mathrm{u} \, \hat{\dot{\mathbf{u}}} \tag{3}$$

$$\dot{\boldsymbol{\varepsilon}} = \nabla \mathbf{N}_\mathrm{u} \, \hat{\dot{\mathbf{u}}} = \mathbf{B}_\mathrm{u} \hat{\dot{\mathbf{u}}} \tag{4}$$

Substituting (Equation 1, Equation 2 , Equation 3) in (Equation 1) and assuming that the stress is constant in each mesh element, the equilibrium equation can be written as

$$\int_\mathrm{V} \mathbf{B}_\mathrm{u}^\mathrm{T} \mathbf{N}_\sigma \mathrm{d}V \, \hat{\boldsymbol{\sigma}} = \int_\mathrm{V} \mathbf{N}_\mathrm{u}^\mathrm{T} \mathbf{F} \mathrm{d}V \tag{5}$$

$$\mathbf{G}\hat{\boldsymbol{\sigma}} = \mathbf{f} \tag{6}$$

where $\mathbf{G}$ is the equilibrium matrix, $\mathbf{f}$ is the external nodal force and $\hat{\boldsymbol{\sigma}}$ are the constant values of stresses inside the mesh elements.The discrete lower bound formulation can be stated as an optimization problem in which the objective is to find the maximum collapse load, such that the system satisfies equilibrium and yield criterion (Camargo et al., 2016)

$$\begin{cases} \text{maximize: } \lambda \\ \text{subjected to: } \mathbf{G}\hat{\boldsymbol{\sigma}} = \lambda \mathbf{f} \\ \mathbf{F}(\hat{\boldsymbol{\sigma}}_{\boldsymbol{i}}) \leq 0, \quad \mathrm{i} = 1 \ldots \text{nelements} \end{cases} \tag{7}$$

where λ is the load factor, and $\mathbf{F}(\hat{\boldsymbol{\sigma}}_{\boldsymbol{i}})$ is the yield criterionvalue for the stress $\hat{\boldsymbol{\sigma}}_{\boldsymbol{i}}$ in the element i.In order to use second-order conic programmingframework, the failure criterion must be cast as a conic quadratic restriction and the Drucker-Prager failure criterion is used for this propose (Makrodimopoulos and Martin, 2006; Carrión et al., 2017)

$$\sqrt{\mathrm{J}_2} + \alpha \, \mathrm{I}_1 - \mathrm{k} \leq 0 \tag{8}$$

where J_2 is the second invariant of the deviator stress tensor, $\mathrm{I}_1$is the first invariant of the stress tensor, and α and k are material parameters that can be determined from the cohesion c and the internal friction angle ϕ of the material

$$\alpha = \frac{\tan\phi'}{\sqrt{9+12\tan^2\phi'}}; \; \mathrm{k} = \frac{3\,c'}{\sqrt{9+12\tan^2\phi'}} \tag{9}$$

The Drucker-Prager criterion can be expressed as a conic quadratic restriction

$$\boldsymbol{\rho} = \mathbf{D}\,\boldsymbol{\sigma} + \mathbf{d} \tag{10}$$

where $\mathbf{D} = \mathbf{D}(\alpha)$ and $\mathbf{d} = \mathbf{d}(\mathrm{k})$ are the matrix and transformation vector, and the elements of $\boldsymbol{\rho}$ belong to second-order quadratic cone (Camargo et al., 2016).

Substituting (Equation 10) in (Equation 7) allows to obtain the conic quadratic form

$$\begin{cases} \text{maximize: } \lambda \\ \text{subjected to: } \mathbf{G}\mathbf{D}^{-1}\boldsymbol{\rho} = \lambda \mathbf{f} + \mathbf{G}\mathbf{D}^{-1}\mathbf{d} \end{cases} \tag{11}$$

The (Equation 11) is solved using MOSEK solver (Mosek, A., 2015).

MATERIAL POINT METHOD

The MPM is a particle method based on the continuum mechanics (Sulsky et al., 1994) that utilizes the advantages of Eulerian and Lagrangian methods. In MPM, the material domain Ω is discretized in a set of Lagrangian points that move through an Eulerian grid. Each material point represents a sub-domain $\Omega_\mathrm{p}$and stores all the relevant

variables such as mass, stress, strain, velocity, and all the internal state variables for history-dependent constitutive modeling. In each MPM computational step all variables in material points are calculated in the grid nodes by using interpolation functions, then the equation of motion is resolved in the grid nodes. The solution is interpolated back to the particles and the grid is reset to the initial configuration (Figure 1).

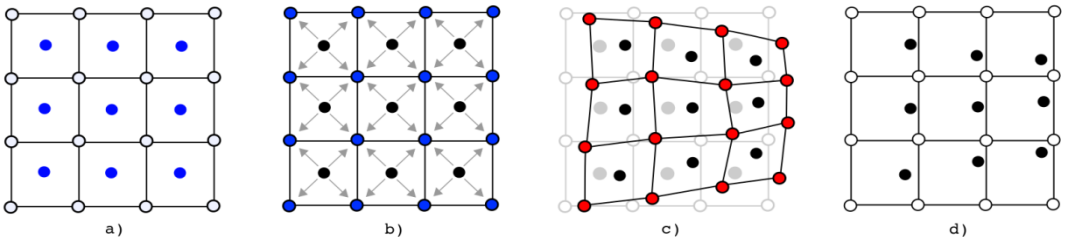

Figure1 Computational cycle in the material point method MPM.

The governing equation of motion of a continuum is the conservation of momentum (Belytschko et al.; 2013):

$$\boldsymbol{\nabla}\cdot\boldsymbol{\sigma}+\rho\mathbf{b}=\rho\,\dot{\mathbf{v}} \tag{12}$$

where$\boldsymbol{\sigma}$is the Cauchy stress tensor, ρ is the mass density, **b** is the body force vector, and$\dot{\mathbf{v}}$is the acceleration vector. The MPM solution is based on weak form of momentum equation (Equation 13) (Zhuang et al., 2016). The week form of equation (Equation 13) is obtained by application of Galerkin method of weighted residual over the entire domain Ωand making use of the integration by parts over the stress term

$$\int_\Omega \rho\ddot{u}_i\delta u_i dV+\int_\Omega \sigma_{ij}\delta u_{i,j}dV-\int_\Omega \rho b_i\delta u_i dV-\int_\Gamma \bar{t}_i\delta u_i dA \tag{13}$$

δuare virtual displacements where$\delta u|_\Gamma=0$, and $\bar{t}$ is the traction in boundary domain Γ.
In the MPM discretization each particle represent a sub-domain, the continuum mass density field can be expressed as

$$\rho(\mathbf{x})=\sum_{p=1}^{n_p} m_p\delta(\mathbf{x}-\mathbf{x}_p) \tag{14}$$

wheren_p are the total number of particles, $m_p$is the mass of particle p, δ is the Dirac delta function, and $\mathbf{x}_p$is the particle positionvector.In order to obtain the discrete equation of motion, the virtual displacement δu_i, the particle displacementu_{ip}, and its derivatives$u_{ip,j}$ are interpolated from the grid nodal values$\delta u_{ip}=N_{Ip}\delta u_{iI}$, $u_{ip}=N_{Ip}u_{iI}$ and $u_{ip,j}=N_{Ip,j}u_{iI}$. Where I is anodal point, and $N_{Ip}=N_I(\mathbf{x}_p)$is the shape function of node Ievaluated in the particle position $\mathbf{x}_p$. Theseinterpolated fields together with the mass density (Equation 14) are replaced in the Equation 13 to obtain the discrete momentum equation at the grid nodes

$$\dot{p}_{iI}=f_{iI}^{int}+f_{iI}^{ext} \tag{15}$$

where p_{iI} is the momentum at grid node I, f_{iI}^{int} and $f_{iI}^{ext}$are the internal and external forces respectively

$$f_{iI}^{int}=-\sum_{p=1}^{n_p} N_{Ip,j}\sigma_{ijp}\frac{m_p}{\rho_p};\ f_{iI}^{ext}=\sum_{p=1}^{n_p} m_pN_{Ip}b_{ip}+\int_\Gamma \bar{t}(x)N_I d\Gamma \tag{16}$$

The stress tensor of a particle σ_{ijp} is obtained by an appropriated constitutive model. To improve computationalefficiency a lumped grid mass matrix is used. The equation of momentum in the grid nodes can be rewritten as:

$$p_{iI}=m_I\dot{u}_{iI} \tag{17}$$

$$m_I=\sum_{J=1}^{n_g} m_{IJ}=\sum_{p=1}^{n_p} m_pN_{Ip} \tag{18}$$

The Equation 17 allows to obtain the accelerations in the grid nodes. The position and velocity of each particle is calculated as:

$$x_{ip} = x_{ip} + \Delta t \sum_I \dot{u}_{iI} N_{Ip} \tag{19}$$

and

$$v_{ip} = v_{ip} + \Delta t \sum_I \ddot{u}_{iI} N_{Ip} \tag{20}$$

The strain increment of the particle is obtained from nodal velocities

$$\Delta\epsilon_{ijp} = \frac{1}{2}\left(N_{Ip,j} v_{iI} + N_{Ip,i} v_{jI}\right)\Delta t \tag{21}$$

The stress increment of the particle is determined from the strain increment using anappropriated constit utive model. To consider the problem of large deformations, the objective Jaumann stress rate $\sigma^{\nabla J}$ is adopted.

$$\boldsymbol{\sigma}^{\nabla J} = \dot{\boldsymbol{\sigma}} - \boldsymbol{\Omega}\,\boldsymbol{\sigma} - \boldsymbol{\sigma}\boldsymbol{\Omega}^{T} \tag{22}$$

where $\boldsymbol{\Omega}$ is the spin tensor

$$\Omega_{ijp} = \frac{1}{2}\left(N_{Ip,j} v_{iI} - N_{Ip,i} v_{jI}\right) \tag{23}$$

In this work theelasto-plastic Drucker-Pragermodel is employed. The model is based on the yield surface (Equation 8). The non-associated flow rule was assumed to consider dilatancy. The plastic potential is defined as

$$\psi^{s} = \sqrt{J_2} + q_\psi I_1 \tag{24}$$

where $q_\psi = \alpha(\psi)$ is determined using the dilation angle ψ (Equation 9).
In the present work the generalized interpolation material point (GIMP) method (Bardenhagen et al.; 2004) is used to reduce the cell crossing noise. The development of the GIPM is beyond the scope of this work.

HETEROGENEOUS SLOPE

In this section we analyze the stability problem of a heterogeneous slope composed of two materials. The slope safety factor and the collapse mechanism are determined using NLA and MPM. The only external force considered is the own weight load of the materials. The Figure 2a shows the definition of the geometry, the materials distribution and the boundary conditions. The boundary conditions are displacements and velocities impeded in three directions in each plane of the slope contour (Figure 2a). The Figure 2b shows the finite element mesh used in NLA with 2912 brick-type elements. The Figure 2.c shows the material points to be used in MPM with 30364 material points.The material properties are shows in Table 1.

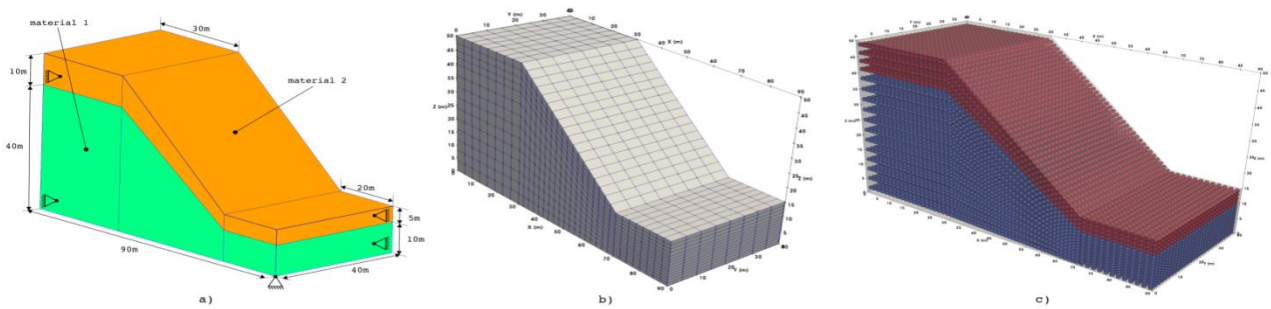

Figure 2 Heterogeneous slope: a)geometry and materials definition;
b) finite element model used in NLA method; c) material points discretization for MPM.

The safety factor is determined by reducing the strength parameters of materials using a scalar value SRF (strength reduction factor). In standard finite elementanalisys the safety factor SF is the maximun SRF for converging solution. In NLA the SF is the SRF that correspond to $\lambda = 1$. In MPM the SF can be determined by the asymptotic value of maximum displacement.

Table 1 Material properties used in heterogeneous slope analysis

Material	E (MPa)	ν (--)	γ (kN/m^3)	c (kPa)	ϕ (°)
1	150.0	0.3	18.0	20.0	30.0
2	150.0	0.3	17.0	15.0	25.0

The Figure 3 shows the results in terms of SRF. For the analysis using NLA, for the standard finite element method FEM with Abaqus, and for the MPM. The results obtained with Abaqus are expressed in terms of dimensionless displacement $\delta = d_{\max} \mathrm{E}/(\gamma \mathrm{H}^2)$, where $d_{max}$is the maximum displacement, E is the Young modulus, γ is the specific weight and H is the height of the slope. In Figure 4 the collapse mechanisms suggested by each method are presented.

Table 2 Slope safety factor and computational time of heterogeneous slope failure.

Method	SF	Time
NLA	1.11	16.0
MPM	1.19	20.0
FEM(Abaqus)	0.98	13986.0

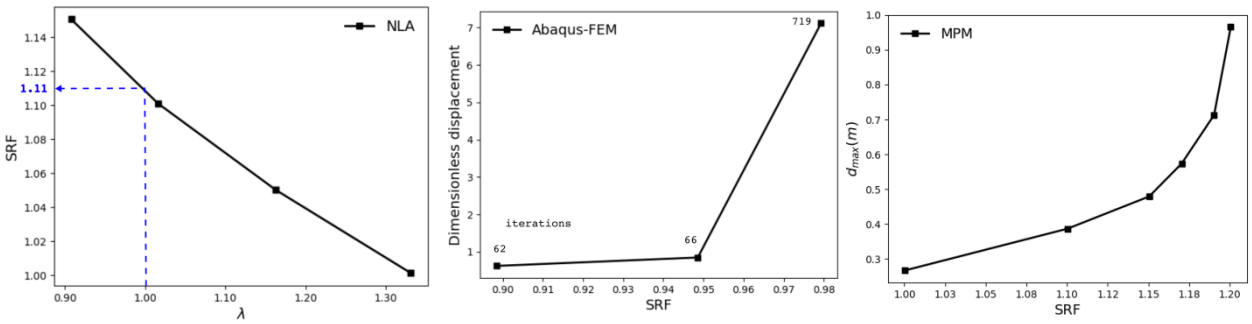

Figure 3 Slope safety factor obtained by different methods: a) SRF values obtained with NLA (Carrión at al., 2017); b) dimensionless displacement values for each SRF obtained with FEM (Abaqus) (Carrión et al., 2017); c) maximum displacement for each SRF obtained with MPM.

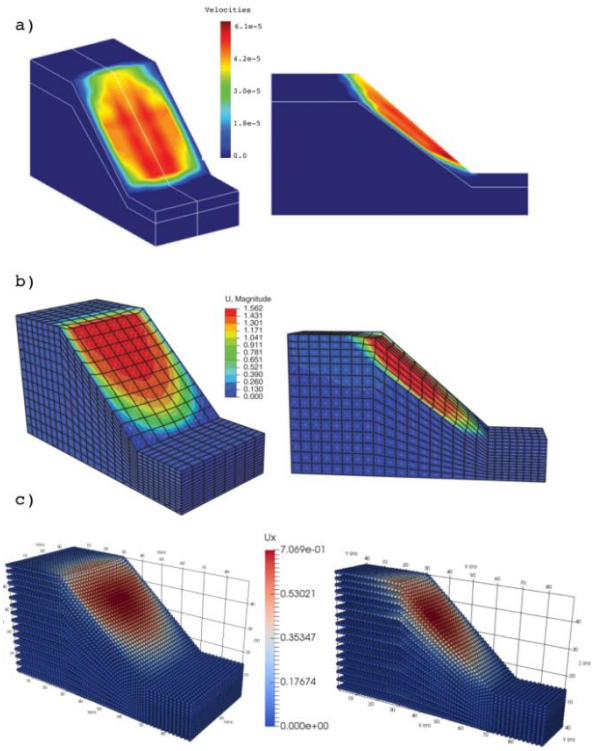

Figure 4 Failure mechanism of the heterogeneous slope.
a) distribution of velocities obtained with NLA for SF = 1.11 (Carrión et al., 2017);
b) distribution of displacements obtained with FEM (Abaqus) for SF = 0.98 (Carrión et al., 2017);
c) displacement field obtained with MPM for SF = 1.19

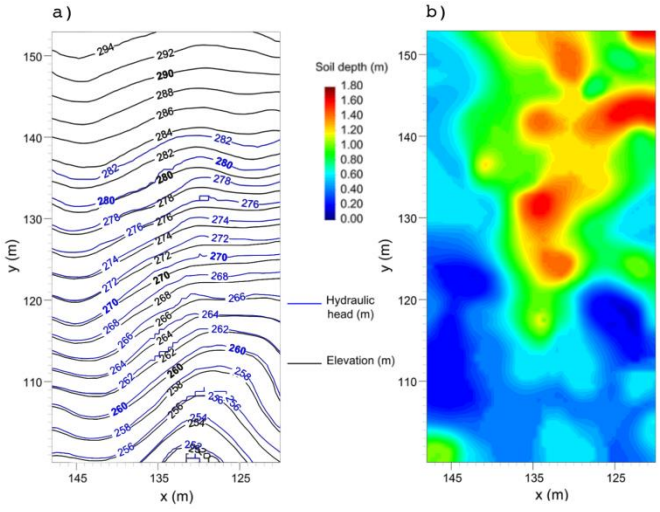

Figure5 Oregon catchment area: a) hydraulic head,
b) soil depth. (Camargo et al., 2016)

CASE STUDY IN THE OREGON CATCHMENT

The next case to be analyzed is the experimental catchment in the Oregon Coast Range. This area collapsed as a large debris flow after an intense rainfall (Borja et al, 2012). Hydrological details of the area are available in (Anderson et al., 1997) (Ebel et al., 2007) and (Montgomery et al., 2009). In this section we present the results of the calculation of the slope safety factor for the experimental catchment in the Oregon Coast Range, and its collapse mechanism obtained by numerical limit analysis (NLA) and material point method (MPM).

The Figure 5 shows the hydraulic head and the soil depth. The pore pressure effects are considered in a non-coupled way through the constitutive relations. The soil depth allows to model the soil layer involved in the failure (Figure 6.a).

Table 3 Strength parameters and unit weight for the Oregon catchment.

E (MPa)	ν (--)	γ (kN/m^3)	c´ (kPa)	ϕ´ (°)
70.0	0.3	13.73	0.9	40.0

Table 4 Comparison of slope safety factor SF.

NLA[1]	LEM[2]	MPM
1.02	1.00	0.97

[1]Numerical Limit Analysis (Camargo et al., 2016)
[2]Limit Equilibrium Method (Milledge et al., 2014)

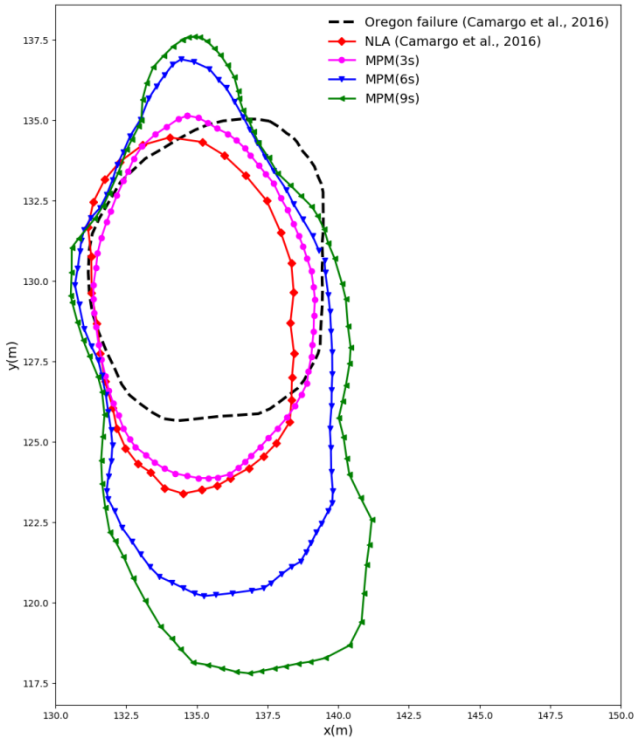

Figure7 Comparison of the scarp zonebetween observed values and the results obtained with NLA and MPM

The Table 4 shows the slope safety factor obtained for the Oregon catchment area. All values are close to 1.0 indicating the imminent collapse for the conditions analyzed.

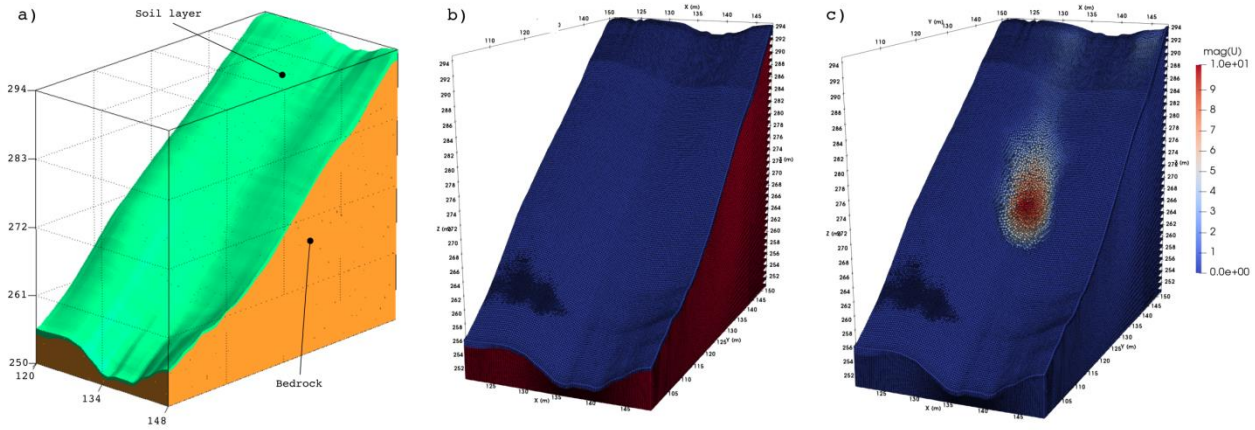

Figure 6 Model of Oregon catchment area: a) geometry and materials definition;
b) Material point discretization with 1.1E6 particles; c) displacement field at 9s after failure

CONCLUSIONS

Numerical limit analysis (NLA) using second-order cone programing and the material point method (MPM) were applied to three-dimensional slope stability analysis. Two cases were analyzed, a heterogeneous slope and the Oregon catchment area. The results show that the slope safety factor and the mechanism of collapse were closebetween the methods used. NLA is highly computationally efficient but did not allow the analysis of post-failurebehavior. The MPM allowed the determination of the slope safety factor and the collapse mechanism more efficiently than the conventional finite element method, and on the other hand allowed the analysis of the post-failure behavior.

REFERENCES

Krabbenhøft, K., Lyamin, A.V. and Sloan, S.W., 2007. Formulation and solution of some plasticity problems as conic programs. International Journal of Solids and Structures, 44(5), pp.1533-1549.

Makrodimopoulos, A. and Martin, C.M., 2006. Lower bound limit analysis of cohesive-frictional materials using second-order cone programming. International Journal for Numerical Methods in Engineering, 66(4), pp.604-634.

Camargo, J., Velloso, R.Q. and Vargas, E.A., 2016. Numerical limit analysis of three-dimensional slope stability problems in catchment areas. Acta Geotechnica, 11(6), pp.1369-1383.Camargo, J., Velloso, R.Q. and Vargas, E.A., 2016. Numerical limit analysis of three-dimensional slope stability problems in catchment areas. ActaGeotechnica, 11(6), pp.1369-1383.

Carrión, M., Vargas, E.A., Velloso, R.Q. and Farfan, A.D., 2017. Slope stability analysis in 3D using numerical limit analysis (NLA) and elasto-plastic analysis (EPA). Geomechanics and Geoengineering, 12(4), pp.250-265.

Mosek, A., 2015. The MOSEK optimization toolbox for MATLAB manual.

Sulsky, D., Chen, Z. and Schreyer, H.L., 1994. A particle method for history-dependent materials. Computer methods in applied mechanics and engineering, 118(1-2), pp.179-196.

Zhang, X., Chen, Z. and Liu, Y., 2016. The material point method: a continuum-based particle method for extreme loading cases. Academic Press.

Belytschko, T., Liu, W.K., Moran, B. and Elkhodary, K., 2013. Nonlinear finite elements for continua and structures. John wiley& sons.

Bardenhagen, S.G. and Kober, E.M., 2004. The generalized interpolation material point method. Computer Modeling in Engineering and Sciences, 5(6), pp.477-496.

Borja, R.I., Liu, X. and White, J.A., 2012. Multiphysics hillslope processes triggering landslides. ActaGeotechnica, 7(4), pp.261-269.

Anderson, S.P., Dietrich, W.E., Montgomery, D.R., Torres, R., Conrad, M.E. and Loague, K., 1997. Subsurface flow paths in a steep, unchanneled catchment. Water Resources Research, 33(12), pp.2637-2653.

Ebel, B.A., Loague, K., Vanderkwaak, J.E., Dietrich, W.E., Montgomery, D.R., Torres, R. and Anderson, S.P., 2007. Near-surface hydrologic response for a steep, unchanneled catchment near Coos Bay, Oregon: 2. Physics-based simulations. American Journal of Science, 307(4), pp.709-748.

Montgomery, D.R., Schmidt, K.M., Dietrich, W.E. and McKean, J., 2009. Instrumental record of debris flow initiation during natural rainfall: Implications for modeling slope stability. Journal of Geophysical Research: Earth Surface, 114(F1).